International Journal of Heat and Mass Transfer xxx (xxxx) 121892

Contents lists available at ScienceDirect

International Journal of Heat and Mass Transfer

journal homepage: www.elsevier.com

Numerical analysis of different mass transfer models for falling film absorbers

P.F. Arroiabe*, Manex Martinez-Agirre, M. Mounir Bou-Ali

Mechanical and Manufacturing Department, Faculty of Engineering, Mondragon Unibertsitatea, Loramendi 4, Arrasate-Mondragon 20500, Gipuzkoa, Spain

ARTICLE INFO

Article history:
Received 28 May 2021
Received in revised form 28 July 2021
Accepted 21 August 2021

Keywords:
Absorption
Falling film
Heat and mass transfer
Numerical analysis
Lithium-bromide

ABSTRACT

Different methodologies have been used in the literature to determine the absorbed vapour mass flux in falling film absorbers. So far, however, there has been little discussion about the impact of different approaches in the numerical models' performance. This study compared different methods for considering absorption in LiBr – H_2O vertical tube-type falling film absorbers operating at both inlet subcooling and equilibrium conditions. This comparison was made based on three different criteria: the way of considering the absorption, the method to determine the absorption rate, and the assumption of the existing type of diffusion at the interface. The influence of the methodology was demonstrated using 2D multiphase CFD model. The effect of different operating conditions on the methods was also examined. Finally, the results of the numerical models were compared with three experimental works, and the most suitable model was chosen, which properly agrees with them.

Nomenclature

A	Area vector
D	Mass diffusion coefficient
D_0	Mass Diffusion coefficient at infinite dilution
$\mathbf{F}_\sigma$	Volumetric surface tension force
g	Gravity acceleration
h	Enthalpy
h_{abs}	Heat of absorption
$\bar{h}_{H_2O}$	Cooling water convection coefficient
$\mathbf{J}_{LiBr}$	LiBr diffusion flux
k	Thermal conductivity
L_c	Characteristic length
$\dot{m}_{abs}$	Absorbed vapour mass flux
Nu	Nusselt number
Pr	Prandtl number
p	Pressure
$\dot{q}_{abs,H_2O}$	Heat flux absorbed by the cooling water
Re	Reynolds number
S	Source term
T	Temperature
V	Volume
v	Velocity vector
x	Longitudinal coordinate
z	Transversal coordinate
Abbreviations	
1D	One-dimensional
2D	Two-dimensional
VOF	Volume of fluid
Greek symbols	
Γ	Mass flow rate per unit length
δ	Solution film thickness
ϕ	Variable
κ	Local surface curvature
μ	Dynamic viscosity
μ^*	Chemical potential
ρ	Density
σ	Surface tension coefficient
Subscripts	
eq	Equilibrium
if	Interface
in	Inlet
l	Liquid
Max	Maximum
min	minimum
out	Outlet
v	Vapour
w	Wall

* Corresponding author.
E-mail address: parroiabe@mondragon.edu (P.F. Arroiabe).

https://doi.org/10.1016/j.ijheatmasstransfer.2021.121892
0017-9310/

α	Volume fraction

1. Introduction

In 2019, the industry sector used 25.8% of the total energy consumption in Europe [1]. Moreover, this sector generates great quantities of waste heat. However, due to its Carnot potential, the industrial area offers a considerable opportunity to reuse a large part of this heat. The choice between different technologies depends, among other factors, on the temperature of waste heat. While mineral processing and metal production sectors offer large waste heat potential at high temperature, in other sectors, such as food and basic chemical, most of the requirement is at low or intermediate temperature [2]. Although mature technologies exist to harness energy at temperatures exceeding 175°C, the research prototypes of most of the technologies to recover waste heat at low temperatures are still under development.

Among them, absorption heat transformers stand out, which can recover 50% of the misuse heat upgrading heat up to 40°C. Due to its low heat and mass transfer coefficients, the absorber is the most critical component in absorption machines. Falling film-type absorber working with $LiBr - H_2O$ binary mixture is the most employed configuration and, it is, consequently, the topic of this study. Principally, there are three types of falling film configurations – horizontal tube, vertical tube, and vertical plate.

Falling film heat exchangers are widely used in absorbers, so several studies have experimentally investigated their heat and mass transfer phenomena. Regarding horizontal tube-type configuration, the influence of operating conditions in plain tubes [3,4], microchannel tubes [5], and advanced surfaces [3,6] was investigated. Notably, the results of these studies presented great differences among them. It follows that these dissimilarities may be due to, among other causes, changes in the wetting area. Also, dry patches were observed in both studies of vertical plates of Kim and Infante Ferreira [7,8]. To improve the wettability, some studies included surfactants in the working mixture, primarily to decrease the surface tension and increase the wettability [9–11]. However, the results showed up to 400% improvement on the heat transfer coefficient. This growth was attributed to the Marangoni convection and the wettability enhancement. Thus, the nature of heat and mass transfer in falling film absorption has remained partially understood.

In contrast, wettability issues could be minimised in the vertical tube-type absorbers. The experimental studies of Medrano et al. [12], Takamatsu et al. [13], and García-Rivera et al. [14] claimed that the solution wetted the whole tube in their corresponding operating conditions. Nevertheless, differences were also found in the mass transfer coefficient among these studies. Therefore, it is imperative to understand locally the mechanisms of heat and mass transfer phenomena in falling film absorption.

Falling film absorption has also been studied using different kinds of models. Killion and Garimella [15] reviewed the heat and mass transfer numerical models of falling film absorption so far. Since then, several studies have analysed the absorption on different configurations using diverse methodologies. While, from the modelling methodology's perspective, these studies can be distinguished as follows: a) analytical models [16,17], b) numerical models based on the Finite Volume Method [18–20], and c) numerical models based on the Lattice Boltzmann Method [21,22], the different modelled configurations are classified into three distinct types: i) horizontal tubes [23,24], ii) flat plates [21,25,26], and iii) vertical tubes [14,27,28]. Most of these models analysed gas or vapour absorption along the interface and mass fraction and temperature profiles within the solution liquid, considering smooth falling film absorption, where operating conditions depended on the application of the absorber. Nevertheless, it is noteworthy that these works employed different approaches and hypotheses to calculate the interface absorption.

The vast majority of these heat and mass transfer models determined the absorption rates using two different methods: a) Fick's law and b) Higbie's penetration theory [29]. Most of the models were formulated using Fick's law, although there are many other works that used Higbie's law [23,30,31]. Both laws have been employed under two different basic diffusion assumptions.

First, many simulations supposed that the mass diffusion occurs in both directions at the interface, liquid-vapour, and vapour-liquid [7,21,32,33]. This assumption means that in a binary mixture, the diffusion flux of both components have opposite directions. In this study, the term 2D diffusion will be used to refer to bidirectional diffusion.

Second, in many real practical cases such as $LiBr - H_2O$ absorbers, the vapour pressure of the absorbent is almost negligible. This means that the absorbent is non-volatile. Consequently, liquid-vapour mass transfer of the absorbent component (LiBr in the case of $LiBr - H_2O$ mixtures) at the interface is lacking. Therefore, mass diffusion only occurs in one direction. In the literature, this phenomenon is referred to as Eckert–Schneider relation [26,33,34], or unidirectional diffusion. Throughout this study, the term "1D diffusion" will refer to this one-way diffusion.

Furthermore, vapour/gas absorption have been considered using different methods in the models. Some studies have used either equilibrium mass fraction [32,35,36] or equilibrium temperature [7,14,33,37] as a boundary condition at the interface. Most of the studies considered one of the mentioned assumptions, which mainly were 2D studies that only modelled the liquid domain. Most of them used nondimensional parameters, as well as nondimensional equations [17,32,33]. Otherwise, constant film thickness was supposed [21].

Other studies determined the interface absorption considering the absorbed mass flux at the interface in the transport equations as a source term [23,31,35,38]. These studies considered both liquid and gas domains, mostly using the Volume of Fluid method (VOF) [39] to track the interface, besides being three-dimensional models.

Recently, Wen et al. [40] reviewed the literature of studies regarding falling film dehumidification and absorption refrigeration based on CFD. Future work suggestions by the authors include the simulation and comparison of the absorption performance with different mass transfer models to increase understanding on coupled heat and mass transfer phenomena.

Overall, the evidence presented in this section suggests that a systematic understanding of how different mass transfer mechanisms contribute to absorption in falling films is still lacking. The quantity of the absorbed vapour at the interface is critical in their performance. Despite the amount of models, so far, there has been little discussion about different methodologies to consider this absorption. Also, no research has been found comparing these diverse methods, and therefore, very little is known about the impact of the methodologies on the results of the model. Thus, this study examines in-depth different methodologies used in the literature to model absorbers to select the most suitable to study heat and mass transfer in $LiBr - H_2O$ falling film absorbers. Vertical tube-type falling film domains were defined to analyse the local heat and mass transfer phenomena and compare the results of the model with the experiments. 2D models were proposed to analyse fundamental local effects on the results of the considered absorption, which were determined using different methodologies, and the impact of different working conditions on them.

2. Numerical model

2.1. Introduction

The description of the numerical model is organised in the following way. First, computational domain and boundary conditions are pre-

sented to continue defining the operating conditions and correlations used to calculate the thermophysical properties. This is followed by the explanation of the governing equations. Finally, different methodologies to consider and determine the absorption in the model, and the hypotheses employed to calculate them are described. Since the other hypotheses are concerned, the numerical model is based on the following assumptions:

1. Equilibrium of the vapour pressure is accepted at the interface.
2. Flow is laminar and the fluid is Newtonian.
3. Duffour and Marangoni effect and the thermodiffusion effect are not considered.
4. Vapour and liquid phases are incompressible.
5. Changes in film thickness due to vapour absorption are not considered.

2.2. Computational domain, boundary conditions, and mesh

Figure 1 shows the layout of a vertical tube falling film absorber (Fig. 1(a)), and the boundary conditions and model discretisation (Fig. 1(b)). The solution, rich in LiBr, enters the domain from the top part to the inner space of the inner tube at specific temperature and mass fractions: T_{in} and w_{in}, respectively. If thermodynamic equilibrium is assumed at the interface, temperature and mass fraction at the inlet are $T_{in} = T_{eq}$ and $w_{in} = w_{eq}$, respectively. If not, the inlet could be subcooled ($T_{in}<T_{eq}$) or overheated ($T_{in}>T_{eq}$). As the solution descends, the vapour is absorbed, decreasing the mass fraction in LiBr at the outlet (w_{out}). From the outer section of the inner tube, water flows in counterflow direction, absorbing the heat generated in the absorption. Through this heat, the temperature of the water at the outlet is higher (T_{w_2}) than at the inlet (T_{w_1}).

Here, an axisymmetric 2D domain was chosen. This means that the absorber has ideal wettability properties, and therefore, the solution wets completely the surface of the tube. From an analytical perspective, Nusselt formulation equates both vertical tubes and flat plates. As vertical plate absorber experimental analyses that guaranteed complete wetting is lacking, the results of the numerical model were compared with the vertical tube LiBr – H_2O absorber experimental investigations. To compare the results of the model and experiments of the literature, different domain sizes and operating conditions were analysed. Because of this, and to optimize computational efforts, the domain changed depending on the analysed solution flow. Table 1 shows the dimensions of the proposed models. In Table 1, the solution film Reynolds number (Re) is defined as:

$$Re = \frac{4\Gamma}{\mu_l}, \tag{1}$$

where Γ is the mass flow rate per unit length, and μ_l is the dynamic viscosity of the solution liquid.

As shown in Fig. 1(b), the grid was refined in z transversal direction within the length s. Its value was determined depending on the theoretical thickness of the liquid film, δ_{Nu}, as $s = 1.1\delta_{Nu}$, which was calculated using the well-known equation of Nusselt [41] (Eq. (2)),

$$\delta_{Nu} = \left[\frac{3\mu_l\Gamma}{\rho_l\left(\rho_l - \rho_v\right)g}\right]^{1/3}, \tag{2}$$

where g is the gravity, and ρ_l and ρ_v are the densities of the solution liquid and the vapour, respectively.

Pressure outlet conditions at 0 Pa (gauge pressure) were assumed on transversal and longitudinal boundaries (z_{Max} and x_{Max}, respectively). In wall side, for z_{min}, no slip boundary condition was set. Furthermore, convection heat transfer condition in the internal surface of the internal tube was considered. As the operating conditions of the compared experimental studies were distinct, the convection heat transfer condition of the model was particularly adjusted to each research study.

Regarding the boundary x_{min}, two different conditions were considered (Eqs. (3a) and (3b)). First, the dimension of the inlet was assumed equal to the relevant theoretical Nusselt film thickness (δ_{Nu}, Eq. (2)), which was determined using the solution flow rate and the properties of each specific case. Thus, this thickness divides the boundary into two different parts depending on z dimension:

$$0 \le z \le \delta_{Nu} \rightarrow \text{ Mass flow inlet} \tag{3a}$$

$$\delta_{Nu} \le z \le 15s \rightarrow \text{ Pressure outlet} \tag{3b}$$

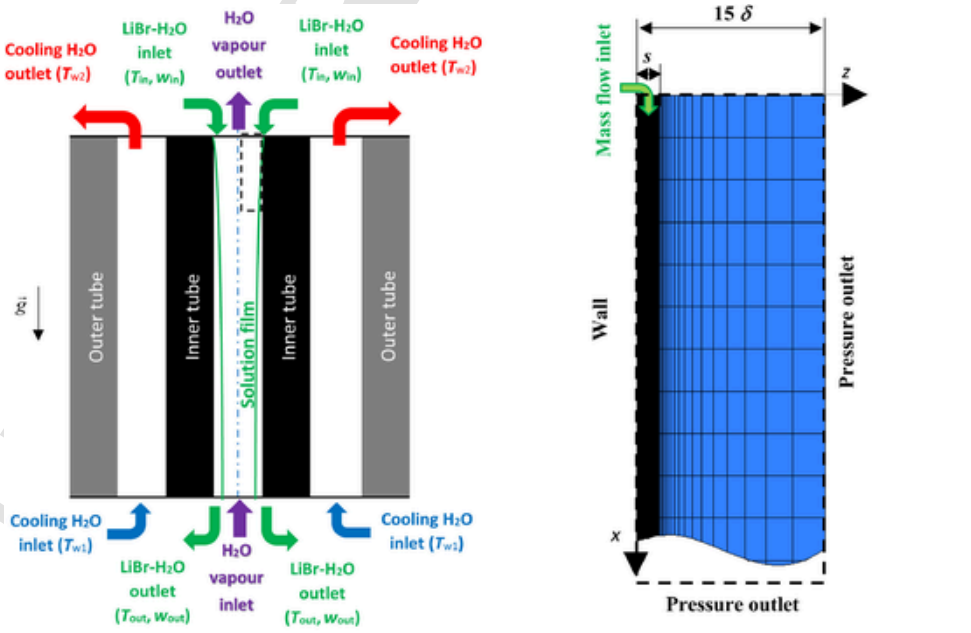

(a) Layout of a vertical tube absorber.

(b) Top detail of the discretisation and boundary conditions of the model.

Fig. 1. Numerical model of the vertical tube absorber.

Table 1
Operating and geometrical conditions used in this study.

Variables/authors	Base case	García-Rivera et al. [14]	Takamatsu et al. [13]	Medrano et al. [12]
Pressure, p/(kPa)	1.30	1.30	1.33	1.30
Inner diameter, d_{in}/(mm)	18.00	18.00	16.05	22.10
Outer diameter, d_{out}/(mm)	22.00	22.00	19.05	26.60
Tube length, x/(mm)	1500	1000	1200	1500
Cooling water convection coefficient, $\bar{h}_{H_2O}$ /($Wm^{-2}K^{-1}$)	6000	2558	1146	9058
Cooling water inlet temperature, T_{in,H_2O}/(°C)	35	30	20, 25	35
Solution Reynolds number, Re	50 – 290	80 – 120	250 – 550	50 – 300
Subcooling degree/(°C)	0	0	0 – 5	10
Inlet mass fraction, $w_{LiBr,in}$	0.6	0.602	0.530	0.600
Minimum Reynolds number, Re_{min}		20	130	40

The mesh was refined in ($0 \le z \le s$) to properly model the heat and mass transfer and the viscous forces. However, the rest of the domain was built with coarser mesh to reduce computational efforts. Details about the computational mesh dimensions are presented in Section 3.1.

2.3. Operating conditions

To validate the proposed methodology, the results of this work were compared with both numerical and experimental studies of vertical absorbers. In the literature, two different techniques were used to determine the equilibrium data at the interface. Consequently, to verify the methodology, two numerical works were chosen for the comparison in this study, one by Yoon et al. [36] and the other by Mittermaier et al. [33]. Yoon et al. [36] considered the equilibrium mass fraction (w_{eq}) regarding pressure and temperature at the interface, while Mittermaier et al. [33] determined the equilibrium temperature (T_{eq}) in function of the pressure and the mass fraction of the interface. Therefore, for this comparison, the same operating conditions of both numerical works were used.

With reference to experimental works, three different researches of vertical tube absorbers were used in the contrast, Medrano et al. [12], Takamatsu et al. [13], and García-Rivera et al. [14]. These works included the study of the minimum $LiBr-H_2O$ Reynolds number to maintain the whole surface covered with liquid film (Re_{min}), which are also included in Table 1. Moreover, convection heat transfer coefficient of the cooling water of the compared experimental work was calculated using Nusselt number (Nu), defined as

$$\mathrm{Nu} = \frac{\bar{h}_{H_2O} L_c}{k}, \tag{4}$$

where $\bar{h}_{H_2O}$ is the convective heat transfer coefficient of the cooling water, L_c the characteristic length, and k the thermal conductivity. Nusselt number depends on the Reynolds number of each experimental test, $Re_{H_2O} = \frac{\rho v L_c}{\mu_l}$, which is calculated using the Dittus–Boelter equation (Eq. (5)) [42] as

$$\mathrm{Nu} = 0.023 {Re_{H_2O}}^{0.8} {Pr_{H_2O}}^{n}, \tag{5}$$

where Pr_{H_2O} is the Prandtl number, and n is an exponent. Table 1 also shows the calculated convective heat transfer coefficients of the cooling water for each experimental work. Thus, the operating conditions of the experimental works differ from each other, and therefore, the models were analysed under different operating conditions.

Furthermore, this study compared different methodologies to consider vapour absorption at the interface. This comparison and the mesh independence study are conducted under specific operating conditions called base case operating conditions. Table 1 shows the operating conditions employed in both studies.

2.4. Thermophysical properties

As in some others models, such as the analytical study of Meyer [16], constant thermophysical properties were assumed. The correlations of density, dynamic viscosity, thermal conductivity, and specific heat were selected from Patterson and Pérez-Blanco [43]. Nevertheless, the mass diffusivity was determined using the relation used by Miller and Keyhani [44]. Concerning the heat of absorption, it was established using the Eq. (6):

$$h_{abs} = h_v - h_l, \tag{6}$$

where h_v and h_l are saturated vapour and liquid enthalpies, respectively. For the enthalpy of water vapour, the tables of Haar et al. [45] were used, while the partial enthalpy of water inside $LiBr-H_2O$ solution was evaluated using the equation proposed by Yuan and Herold [46]. The relationship of the heat of absorption with temperature for a known mass fraction under the conditions of this study is almost linear. Similarly, for a known temperature, the heat of absorption is a quadratic function of the LiBr mass fraction. Consequently, these relationships were used to determine the heat of absorption regarding temperature and LiBr mass fraction.

2.5. Governing equations

To solve the governing equations, Ansys Fluent 2021 R1 software based on the Finite Volume Method was used. The continuity (Eq. (7a)), momentum (Eq. (7b)), and energy (Eq. (7c)) equations were solved for the liquid–vapour mixture. The heat generated due to the water vapour absorption was considered in the source term S_Q (Eq. (7c)).

$$\frac{\partial \rho}{\partial t} + \nabla \cdot (\rho \mathbf{v}) = 0, \tag{7a}$$

$$\frac{\partial}{\partial t}(\rho \mathbf{v}) + \nabla \cdot (\rho \mathbf{v}\mathbf{v}) = -\nabla p + \nabla \cdot (\mu \nabla \mathbf{v}) + \rho \mathbf{g} + \mathbf{F}_\sigma, \tag{7b}$$

$$c_p \frac{\partial}{\partial t}(\rho T) + c_p \nabla \cdot (\rho \mathbf{v} T) = \nabla \cdot (k \nabla T) + \sum_{i=1}^{2} \left(h_i \mathbf{J}_i\right) + S_Q. \tag{7c}$$

In the energy equation, i refers to ith specie, h is the sensible enthalpy, $\mathbf{J}_i$ is the diffusion flux of species, and $\mathbf{F}_\sigma$ the volumetric surface tension force. The latter, was calculated using continuum surface force model proposed by Brackbill et al. [47], as follows

$$\mathbf{F}_\sigma = \sigma \frac{\rho \kappa \nabla \alpha}{0.5\left(\rho_l + \rho_v\right)}, \tag{8}$$

where σ is the surface tension coefficient, κ is the local surface curvature, and α is the volume fraction of liquid phase. This volume fraction was considered using the volume fraction equation based on the VOF method proposed by Hirt and Nichols [39] as:

$$\frac{1}{\rho_l}\left[\frac{\partial}{\partial t}\left(\alpha_l \rho_l\right) + \nabla \cdot \left(\alpha_l \rho_l \mathbf{v}_l\right) = 0\right], \tag{9}$$

In contrast, the volume fraction of the vapour phase was determined considering that both volume fractions sum to unity. VOF method employs the volume fraction, α, to identify each phase. If $\alpha = 0$, the cell belongs to the phase gas/vapour, while if $\alpha = 1$, the cell is in the liquid phase. However, if it is between both values, it corresponds to the interface. As in this study vapour and liquid phases were considered, the interface coincides with the cell where the line of constant value of

$\alpha = 0.5$ passes, that is, when the value $\alpha = 0.5$ is between the values of the faces of the cell. In Fig. 2, uppercase letters represent cell centroids and lowercase letters the faces. Thus, here the interface constitutes the cell P.

Regarding the mass diffusion, the mass transfer promoted by the LiBr diffusion inside the solution film was also considered using the multiphase species conservation equation as follows:

$$\frac{\partial}{\partial t}\left(\alpha_l \rho_l w_{\mathrm{LiBr}}\right) + \nabla\cdot\left(\alpha_l \rho_l \mathbf{v}_l w_{\mathrm{LiBr}}\right) = -\nabla\cdot \alpha_l \mathbf{J}_{\mathrm{LiBr}} + \alpha_l S_{\mathrm{LiBr}}, \tag{10}$$

where S_{LiBr} is the LiBr source term and $\mathbf{J}_{\mathrm{LiBr}}$ the diffusion flux of LiBr. As in the VOF equation, the mass fraction of the water was estimated assuming that the mass fractions of the binary solution sum to unity. Here, the diffusion flux of LiBr was evaluated using Fick's first law (Eq. (11)):

$$\mathbf{J}_{\mathrm{LiBr}} = -\rho_l D \nabla w_{\mathrm{LiBr}}. \tag{11}$$

Most of the studies considered the commonly used vapour pressure equilibrium to calculate properties at equilibrium conditions at the interface. According to Yuan and Herold [46], when the interface reaches equilibrium, the chemical potential of the water in the solution ($\mu^*_{l,\mathrm{H_2O}}$) is equal to the chemical potential of the vapour ($\mu^*_{g,\mathrm{H_2O}}$) at equilibrium conditions.

$$\mu^*_{l,\mathrm{H_2O}}(w,T,p) = \mu^*_{g,\mathrm{H_2O}}(T,p). \tag{12}$$

Based on Eq. (12), the relationship between equilibrium temperature (T_{eq}) and mass fraction (w_{eq}) for each working pressure can be determined using Newton–Raphson method. As this relationship is almost linear, a linear equation was employed, for example, as in the studies of Hofmann and Kuhlmann [26] and Meyer [16]. Here, the chemical potential of the water vapour was calculated using the correlations of Ziegler and Trepp [48], while the chemical potential of the water in the binary solution was determined via Yuan and Herold correlations [46].

The pseudo transient solution method was used with the coupled pressure-velocity scheme to solve the equations. PRESTO! pressure discretization method was employed, and second order upwind was used to solve energy, momentum and species transport equations. Furthermore, in this case the compressive algorithm was used to capture the interface.

2.6. Methodologies to consider the absorption

Source terms S_{LiBr} and S_Q were determined depending on the used approach to consider the absorption. All of them were considered in the model using User Defined Functions. In this study, different methodologies were employed based on three different criteria.

1. The method to determine the absorption rate.
   (a) Fick's law.
   (b) Higbie's law [29].
2. The assumption of the existing type of diffusion at the interface.
   (a) 2D diffusion.
   (b) 1D diffusion.
3. The way of considering the absorption.

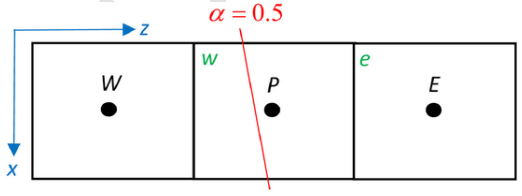

Fig. 2. Schematic of the indices used for cells and faces at the interface.

   (a) Imposing thermodynamic equilibrium conditions (temperature or mass fraction) at the interface.
   (b) Without imposing, considering the absorption via source terms that depend on the absorbed vapour mass flux.

The first criterion is associated with the method to determine the absorption rate: a) Fick's law, or b) Higbie's law [29]. The second criterion relates to assumption of the existing type of diffusion at the interface: i) 2D diffusion or ii) 1D diffusion. Finally, the third criterion is connected with the way to consider the absorption: 1) imposing thermodynamic equilibrium conditions (temperature or mass fraction) at the interface, or 2) without imposing, considering the absorption via source terms that depend on the absorbed vapour mass flux.

Considering the first two criteria, four different ways to quantify the mass transfer at the interface due to vapour absorption were employed. When Fick's law was used and 2D diffusion was assumed at the interface, as Fick's law assumes that the mass transfers of the species are opposite for a binary mixture, the local mass flux was calculated directly with Fick's law:

$$\dot{m}_{\mathrm{abs,\ Fick\ 2D}} = -\rho_l D_{\mathrm{if}}\left[\frac{\partial w_{\mathrm{LiBr}}}{\partial n}\right]_{\mathrm{if}}, \tag{13}$$

where D_{if} is the diffusion coefficient, and $\left[\frac{\partial w_{\mathrm{LiBr}}}{\partial n}\right]_{\mathrm{if}}$ the derivative of the mass fraction in the direction normal to the interface. Taking the schematic shown in Fig. 2 as an example, the derivative could be determined as:

$$\frac{w_{\mathrm{LiBr},P} - w_{\mathrm{LiBr,W}}}{\Delta z_{P,W}}. \tag{14}$$

In contrast, when 1D diffusion was supposed, the mass balance at the interface changes. Similar to Mittermaier and Ziegler [49], the absorbed mass flux was determined with:

$$\dot{m}_{\mathrm{abs,\ Fick\ 1D}} = -\frac{\rho_l D_{\mathrm{if}}}{w_{\mathrm{LiBr,if}}}\left[\frac{\partial w_{\mathrm{LiBr}}}{\partial n}\right]_{\mathrm{if}}. \tag{15}$$

For penetration theory of Higbie [29], notably, some studies used the expression suggested to calculate the average absorbed mass flux over a given flow length to consider the local mass flux. The original formulation of the local mass flux assumes 2D diffusion [50], as

$$\dot{m}_{\mathrm{abs,\ Higbie\ 2D}} = \rho_l\sqrt{\frac{D_{\mathrm{if}}u_{\max}}{\pi x}}\left(w^{\mathrm{eq}}_{\mathrm{LiBr,\ if}} - w_{\mathrm{LiBr},\infty}\right), \tag{16}$$

as where $u_{\max}$ is the maximum velocity at the interface, x is the flow length, and $w^{\mathrm{eq}}_{\mathrm{LiBr,\ if}}$ and $w_{\mathrm{LiBr},\infty}$ are the equilibrium mass fraction at the interface and the mass fraction of the solution adjacent to the wall, respectively. Equation (16) assumes that the contact time is $x/u_{\max}$. Originally, this study also presumed 1D diffusion at the interface using this penetration theory. For this assumption, the absorbed mass flux was calculated as:

$$\dot{m}_{\mathrm{abs,\ Higbie\ 1D}} = \frac{\rho_l}{w_{\mathrm{LiBr,\ if}}}\sqrt{\frac{D_{\mathrm{if}}u_{\max}}{\pi x}}\left(w^{\mathrm{eq}}_{\mathrm{LiBr,\ if}} - w_{\mathrm{LiBr},\infty}\right). \tag{17}$$

Regarding the third criterion, when vapour pressure equilibrium conditions are not imposed at the interface, S_{LiBr} was associated with the local absorbed mass flux ($\dot{m}_{\mathrm{abs}}$) and the interfacial area density (A_{if}) as:

$$S_{\mathrm{LiBr}} = \dot{m}_{\mathrm{abs}}\cdot A_{\mathrm{if}}, \tag{18}$$

where A_{if} was determined using Eq. (19):

$$A_{\text{if}} = \frac{|\mathbf{A}|}{V} \tag{19}$$

Here, $\mathbf{A}$ denotes the vector normal to the interface of the area of the cell, and V the volume of the cell.

Once the source term was known, the volumetric heat source S_Q was calculated using heat of absorption:

$$S_Q = S_{\text{LiBr}} h_{abs}. \tag{20}$$

Thus, depending on the used law (Fick or Higbie) and the diffusion hypothesis (1D or 2D), four different values of the absorbed mass flux could be considered when equilibrium conditions are not imposed.

Conversely, many studies, as they only considered the liquid phase, imposed the equilibrium conditions at the interface as a boundary condition. However, in this study, as both phases were studied, the interface does not match with the boundary. So, the so-called "internal boundary condition" method suggested by Patankar [51] was used to impose thermodynamic equilibrium conditions at the interface using the linearisation concept of the source term.

Nevertheless, as mentioned in Section 1, some authors imposed the equilibrium temperature at the interface, while others used the equilibrium mass fraction. Consequently, the manner of calculating it differs in both cases. Notably, all of them used Fick's law, assuming 1D or 2D diffusion. As no study has been found imposing equilibrium conditions using Higbie's law, in this study, Higbie's law was not considered when equilibrium conditions were imposed.

On the one hand, when the equilibrium temperature was assumed at the interface, it was determined using Dhring equation. So, using the nomenclature of Fig. 2, the imposed temperature at the interface was determined as

$$T_P = T_{eq}\left(p, w_P\right), \tag{21}$$

where T_P is the temperature at the interface, and T_{eq} is the equilibrium temperature at a given pressure p and mass fraction w_P. The mass fraction at the interface was determined coupling the energy balance.

$$k\left(\frac{dT}{dn}\right)_{\text{if}} = \dot{m}_{\text{abs}} h_{\text{abs}}\left(T_{\text{eq}}\left(p, w_P\right), w_P\right). \tag{22}$$

Nevertheless, depending on the diffusion hypothesis, the absorbed mass expression is different and, consequently, the mass fraction. Assuming 2D diffusion, the mass fraction at the interface ($w_{\text{LiBr,P,Fick 2D}}$) is determined using Eq. (23)

$$k\frac{T_{\text{eq}}\left(p, w_P\right) - T_W}{\Delta z_{P,W}} = -\rho_l D_{\text{if}} \frac{w_{\text{LiBr},P,\text{Fick 2D}} - w_{\text{LiBr,W}}}{\Delta z_{P,W}} h_{\text{abs}}\left(T_{\text{eq}}\left(p, w_P\right), w_P\right).($$

Alternatively, considering 1D diffusion at the interface, Eq. (24) was used:

$$k\frac{T_{\text{eq}}\left(p, w_P\right) - T_W}{\Delta z_{P,W}} = -\frac{\rho_l D_{\text{if}}}{w_{\text{LiBr},P,\text{Fick 1D}}} \frac{w_{\text{LiBr},P,\text{Fick 1D}} - w_{\text{LiBr},W}}{\Delta z_{P,W}} h_{\text{abs}}\left(T_{\text{eq}}\left(p, w_I\right.\right.$$

On the other hand, when equilibrium mass fraction was imposed, it was estimated regarding the pressure and temperature at the interface

$$w_{\text{LiBr},P} = w_{\text{LiBr,eq}}\left(p, T_P\right). \tag{25}$$

As in the other case, two different expressions can be developed to determine the value of the temperature for 2D diffusion ($T_{P,\text{Fick 2D}}$, Eq. (26a)), and for 1D diffusion ($T_{P,\text{Fick 1D}}$, Eq. (26b)).

$$k\frac{T_{P,\text{Fick 2D}} - T_W}{\Delta z_{P,W}} = -\rho_l D_{\text{if}} \frac{w_{\text{LiBr,eq}}\left(p, T_P\right) - w_{\text{LiBr},W}}{\Delta z_{P,W}} h_{\text{abs}}\left(T_{\text{eq}}\left(p, w_P\right), w_P\right)(2$$

$$k\frac{T_{P,\text{Fick 1D}} - T_W}{\Delta z_{P,W}} = -\frac{\rho_l D_{\text{if}}}{w_{\text{LiBr,eq}}} \frac{w_{\text{LiBr,eq}}\left(p, T_P\right) - w_{\text{LiBr},W}}{\Delta z_{P,W}} h_{\text{abs}}\left(T_{\text{eq}}\left(p, w_P\right), w_{P,}\right.$$

Thus, depending on the chosen diffusion hypothesis, the law used to determine the absorption rate and the chosen equilibrium variable, the imposed properties could be calculated using four different equations (Eqs. (23), (24), (26a), and (26b)). These calculated temperatures and mass fractions were set as desired variable in the source term linearised equation as in [51] to determine the source term of the energy conservation equation (Eq. (7c) and species equation (Eq. (10)).

In summary, when equilibrium conditions were not imposed at the interface, the source terms were considered depending on the absorbed mass flux. Based on the chosen diffusion hypothesis and law, four different equations could be employed to calculate this absorbed flux (Eqs. (13), (15), (16), and (17)). Conversely, when equilibrium was imposed, the method suggested by Patankar [51] was used to determine the source term of energy and species. In this method, four different expressions (Eqs. (23), (24), (26a), and (26b)) were also employed to calculate the desired values, depending on the adopted methodology and hypothesis.

3. Results and discussion

The results are organised as follows. First, the effect of the mesh is checked. Using the chosen independent mesh, the reliability of the model is examined by comparing the results of this study to those of the literature. Then, the influence of different methodologies to determine and consider the absorption is evaluated. Once the desired approaches are selected, the influence of different operating conditions on the chosen methods is evaluated. Finally, the results of the proposed numerical methodology are compared with three experimental studies in the literature.

3.1. Mesh independence

First, the mesh independence of the model for the different methods to consider absorption described in Section 2.6 was studied. Two different Reynolds numbers were checked. These and the other selected operating conditions are presented in Table 1 (base case). Particularly, the influence of the following variables was studied: i) the number of elements of the liquid film in the z transversal direction: $25 \leq N_{\text{transversal}} \leq 200$ and, ii) the number of elements in the x longitudinal direction: $500 \leq N_{\text{longitudinal}} \leq 10000$.

The analysis was organised based on the two studied different methods to determine the absorbed mass flux: Fick 1D and Higbie 1D. For Fick 1D, two distinct ways to consider absorption are studied: i) imposing the equilibrium mass fraction at the interface, and ii) without imposing. As mentioned in Section 2.6, in this study, imposing equilibrium conditions method using Higbie's law was not studied.

Figure 3 compares the local absorbed vapour mass flux along the flow length x using the method Fick 1D imposing the mass fraction for different grids ($N_{\text{transversal}} \times N_{\text{longitudinal}}$) and two different Reynolds numbers: $Re = 290$ (Fig. 3(a)) and $Re = 50$ (Fig. 3(b)). For the selection criterion, the difference in percentage of the absorbed mass flux of the specific grid, compared to the densest one, was used.

When $Re = 290$ (Fig. 3(a)), although the results for different grids are similar, the increasing absorption velocity close to the inlet is higher as the mesh is thinner. As the difference is below 1%, the mesh was considered independent when $N_{\text{transversal}} = 100$. In contrast, when $Re = 50$ (Fig. 3(b)), the increase in absorption close to the inlet and the maximum peak is higher than when $Re = 290$. Both are lower as thinner is the mesh, although differences are not great. However, comparing with $Re = 290$, the fall is higher after the maximum flux. Also, when $Re = 50$, the number of elements to get independent mesh is higher than for $Re = 290$, specifically $N_{\text{transversal}} = 150$.

Once set the transversal direction, the analysis of the longitudinal direction was conducted. Figure 4 shows the comparison regarding the number of longitudinal elements of the absorbed mass flux using Fick 1D, imposing method for two different cases: $Re = 290$ (Fig. 4(a)) and $Re = 50$ (Fig. 4(b)). Each case maintains constant the transversal number of elements determined above. What stands out in Fig. 4 is that the number of longitudinal elements has virtually no influence on both Reynolds numbers. Particularly, the difference in both cases is below 0.25%.

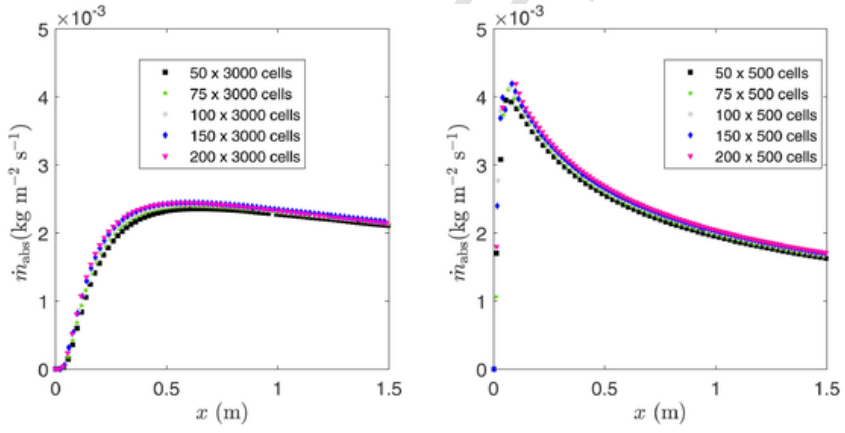

Fig. 3. Effect of the mesh in the transversal direction on the local absorbed vapour mass flux along the flow length using Fick 1D method, imposing the equilibrium mass fraction for different Reynolds numbers.

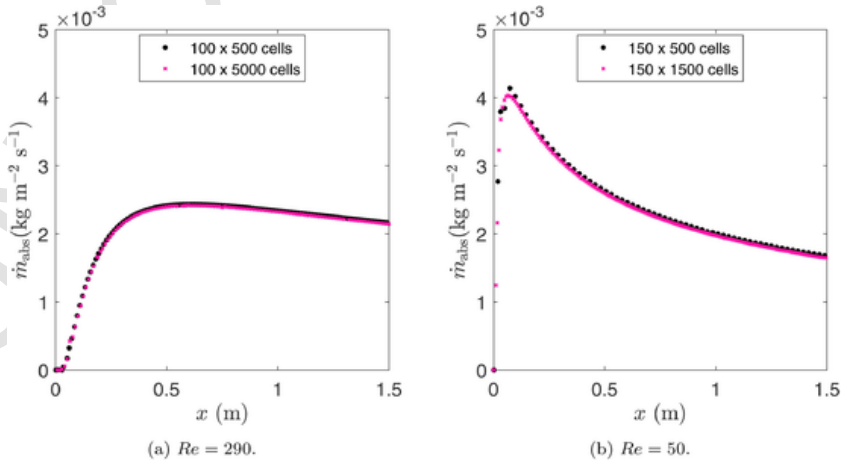

Fig. 4. Effect of the mesh in the longitudinal direction on the local absorbed vapour mass flux along the flow length using Fick 1D method, imposing the equilibrium mass fraction for different Reynolds numbers.

After studying the imposing method, the mesh dependency using no imposing Fick 1D method was revised. From Fig. 5(a), a grid of 100×500 provides independent results.

Finally, Higbie 1D without imposing method was analysed. This was done because the number of elements of both methods (Fick and Higbie) does not necessarily have to be the same. Figure 5(b) presents the local absorbed mass flux for different grids when $Re = 50$. It is apparent from Fig. 5(b) that the mesh has no influence within the studied range when the method Higbie 1D without imposing conditions is used. Table 2 summarises the required minimum cell numbers in the transversal and longitudinal direction, beyond which the effect of the mesh in the results of the model will be negligible for both models (Fick 1D and Higbie 1D), and for different Reynolds numbers.

This section suggests that a higher density mesh is needed when the absorbed mass flux is calculated using Fick's law. Furthermore, here, the results demonstrated that mesh requirements depend on the Reynolds number. The lower the Reynolds number, the higher the number of cells required in the transverse direction of the film. In the longitudinal direction, however, the number of cells required is not as constraining. This might be because the gradients of the different variables (velocity, temperature, mass fraction, etc) are smaller in this direction. Together, this study illustrates that when using the method Higbie 1D, as it is not necessary to capture the mass fraction gradient at the interface, mesh requirements are lower, reducing considerably computational efforts. Considering all this evidence, to minimise computational efforts it was decided to use two different meshes for each method for the analysed Reynolds range: Fick: 150×500 cells; and Higbie: 50×500 cells.

3.2. Validation of the model

Once the computational mesh was selected, to validate the model, the results of the model of the present study were compared with the results of the model of Yoon et al. [36] and Mittermaier et al. [33]. Both works assumed bidirectional diffusion at the interface, they determined the absorbed mass flux via Fick's law, and they imposed equilibrium conditions at the interface. However, while Yoon et al. [36] imposed the equilibrium mass fraction, Mittermaier et al. [33] imposed equilibrium temperature. Hence, the mass fraction at the interface was compared with the former. In contrast, the comparison with Mittermaier et al. was made based on temperature. However, they only showed interface temperature profiles for inlet subcooled conditions, not for saturated conditions. Despite this, as they presented transversal temperature profiles for inlet saturated conditions, the comparison was made based on this temperature.

For this purpose, Fig. 6(a) presents the comparison of the interface mass fraction along the longitudinal direction between the model of this study and those of Yoon et al. [36]. Besides, Fig. 6(b) shows temperature profile in the transversal direction (in this case, using dimensionless transversal coordinate z/δ), when $x = 0.031$ m between this analysis and those of Mittermaier et al. [33]. The operating conditions of both models are identical to the authors. From the results of Fig. 6, it is evident that the results of the present model are like those of the numerical studies.

3.3. Study of different methodologies to consider the absorption

Once the numerical methodology was validated, the comparison between the different methodologies presented in Section 2.6 was analysed. Figure 7 shows local absorbed mass flux over flow length when local $Re = 50$ and $Re = 290$ for the Fick approach and two different methods to consider the absorption: imposing and not imposing equilibrium mass fraction at the interface.

Observably, when Fick 1D was considered, the local mass flux for imposing and not imposing methods almost coincides. Nevertheless, this similarity is absent when the absorption was estimated using Fick 2D. Here, it is apparent from Fig. 7 that the absorbed mass flux is higher when equilibrium is not imposed at the interface. Therefore, for $Re = 50$, the absorption consideration procedure (imposing and not imposing) lacks significant influence for Fick 1D, whereas it has a significant impact when considering the hypothesis of Fick 2D (Fig. 7).

A similar effect was observed for the chosen mass diffusion assumption. When mass fraction was imposed, the diffusion assumption has a major influence on the absorbed mass (Fig. 7), while its transcendence is almost imperceptible when the equilibrium mass fraction is not imposed at the interface for $Re = 50$. However, this difference varies with the Reynolds number. For example, for $Re = 290$, there is a slight increase in the local absorbed mass flux when 1D diffusion is assumed.

To understand the cause for this disparity, Fig. 8(a) illustrates the mass fraction profile over transversal direction (z) at the exit of the vertical tube ($x = 1.5$ m), while Fig. 8(b) presents the mass fraction at the interface along the flow length, both for $Re = 50$ and imposing conditions.

Following the results of Fig. 8(a), the decline in the mass fraction along the transversal direction, and therefore, the absorption, is higher when 2D diffusion is assumed. Contrarily, this is at odds with the observation in Fig. 7, since the local absorbed vapour mass flux is higher for Fick 1D than for Fick 2D when equilibrium conditions are imposed. This contradiction may be because, when equilibrium conditions are forced at the interface, the absorbed vapour mass flux quantity is not included directly in the source term. Instead, the water quantity that is

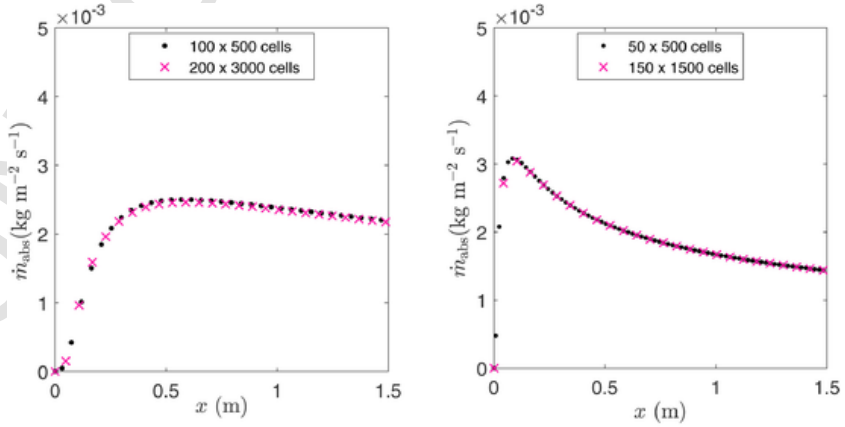

(a) $Re = 290$ Fick 1D. (b) $Re = 50$ Higbie 1D.

Fig. 5. Local absorbed mass flux at the interface for different Reynolds numbers and methods without imposing equilibrium conditions.

Table 2
Mesh number requirements for the studied methods and Reynolds numbers.

	Fick 1D		Higbie 1D	
	Transversal	Longitudinal	Transversal	Longitudinal
Re = 50	150	500	50	500
Re = 290	100	500	50	500

transferred into the solution liquid depends on the diffusion flux of species ($\mathbf{J}_{\mathrm{LiBr}}$, Eq. (11)) of the species equation (Eq. (10)), which is based on Ficks law and assumes 2D diffusion.

Thus, as the evaluated absorption in the 1D imposing case is larger (Fig. 7), the generated heat also increases, rising the temperature at the interface. Consequently, the equilibrium mass fraction (determined by Dühring equation) is larger for 1D than for 2D. This increase in the mass fraction induces a reduction of mass fraction gradient, lowering the vapour mass absorption into the film. Consequently, although for imposing Fick 1D the estimated value of the absorbed mass is superior, the water quantity that goes into the film considered by the model is lower. This also induces a higher LiBr mass fraction in the outlet for Fick 1D. Therefore, the proposed Fick method imposing the mass fraction does not correctly represent the 1D diffusion hypothesis. Thus, this method is excluded from this study.

For Fick without imposing method, Fig. 8(c) shows the results of the mass fraction profile in the transversal (z) direction at the tube outlet ($x = 1.5$ m) for $Re = 50$. What is interesting about the data in Fig. 8(c) is that the mass fraction profile is almost equal for both hypotheses (2D and 1D). These results are comparable to those presented in Fig. 7 since the local mass flux obtained in both cases is similar.

The difference when compared to the imposed method may be that when conditions are not imposed, the source terms of the conservation equations are directly related to the determined mass flux. As can be observed, comparing Eqs. (13) and (15), the difference resides in the denominator of the right-hand side. Therefore, for the same mass fraction profile in the liquid, the absorbed mass flux is higher for Fick 1D than for Fick 2D and, consequently, the source terms. On the one hand, because of the augment of generated heat and temperature, the mass fraction at the interface increases. On the other hand, because of the growth in the absorbed water, the LiBr mass fraction decreases. Both effects induce lower mass fractions at the interface. Thus, when $Re = 50$, the increase in the mass flux due to 1D hypothesis is neutralised by the decline in the mass fraction gradient, achieving similar absorption levels in both assumptions (1D and 2D). When $Re = 290$, the behaviour is similar, but the differences are slightly higher.

Finally, the comparison was extended to Higbie's penetration theory, as commented above, without imposing conditions. Figure 9 presents the comparison between the different diffusion assumptions of the local mass flux along the flow length when $Re = 50$.

It is apparent in Fig. 9 that the hypothesis greatly affects the absorption, being considerably higher for 1D diffusion. In Higbie's law, the absorption does not depend on the mass fraction. Consequently, the decrease in LiBr mass fraction close to the interface is not directly considered in the absorption. Thus, the diffusion assumption has a significant effect, being greater for unidirectional diffusion.

Overall, this subsection demonstrates that the methodology and the diffusion hypothesis used to determine and consider the absorption affect in the results of the model. Furthermore, the results illustrated that, when equilibrium conditions are imposed at the interface, the calculated absorption rate is not equal to the vapour introduced in the model into the liquid film. Therefore, this method was discarded. Also, the results of the models without imposition showed that the diffusion assumption greatly impacts the absorption using Higbie's law, while it almost does not affect Fick method. Nevertheless, as the LiBr liquid–vapour diffusion at the interface is negligible, only 1D diffusion assumption will be considered in the following models. Thus, since Fick 1D and Higbie 1D methods may be preferable to reproduce the nature of the diffusion at the interface, in the subsequent analyses, these two methods without imposing the equilibrium conditions are applied in the models. Nevertheless, it should be noted that the results obtained using Fick 2D without imposition method were similar to those of Fick 1D without imposition (Figs. 7 and 8(c)), and therefore, it could also be a valid method.

3.4. Influence of the operating conditions on the selected methodologies

After discussing the suitability of each method, the effect of different operating conditions, such as solution Reynolds number, cooling liquid convection heat transfer, and solution inlet mass fraction was investigated.

Figure 10 shows the average value of absorbed mas flux (Fig. 10 (a)) and the average value of the absorbed heat flux by the cooling fluid (Fig. 10(b)), both were determined using Fick 1D and Higbie 1D methods, for the range $50 \leq Re \leq 290$. Operating conditions are the same as in Section 3.3.

As Fig. 10 illustrates, both methods show the same trend. For absorbed mass flux, both reach a peak when $Re = 75$ (Fig. 10(a)). For heat flux, the higher the Reynolds number, the higher the heat flux (Fig. 10 (b)). However, the values obtained using Fick 1D are larger, and basi-

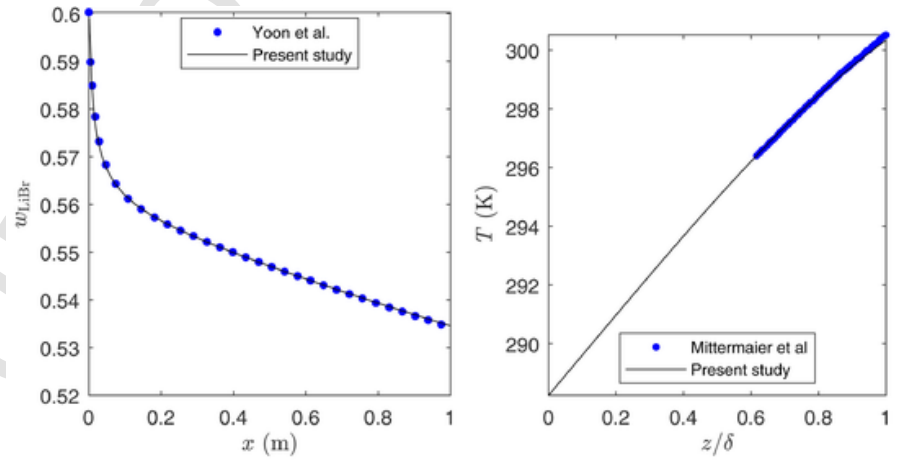

(a) Yoon et al. [36], LiBr mass fraction profile at the interface along the flow length.

(b) Mittermaier et al. [33], temperature profile over dimensionless transversal coordinate (z/δ).

Fig. 6. Comparison between the present study and two numerical analyses of the literature.

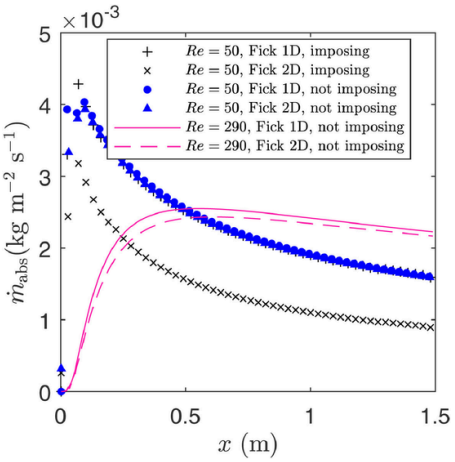

Fig. 7. Comparison of the local absorbed mass flux along the flow length for Fick 1D and Fick 2D imposing and not imposing equilibrium mass fraction when $Re = 50$ and $Re = 290$.

cally, the difference between both methods remains constant. To further study these differences, Fig. 11 presents the local absorbed mass flux for different Reynolds numbers considering Fick 1D (Fig. 11(a)) and Higbie 1D (Fig. 11(b)).

Figure 11 illustrates that for low Reynolds numbers, the maximum peak of mass flux is larger for both methods because the lower the Reynolds number, the lower are the solution mass flow and the film thickness. Consequently, the temperature and the mass fraction are minor for lower Reynolds number, which increase the determined mass flux. Also, as the thermal boundary layer develops earlier, the maximum peak occurs at lower flow length as the Reynolds number is smaller. However, the higher the Reynolds number, the lower the maximum mass flux peak and this is located at a longer flow length. In contrast, at low Reynolds number, there is a noticeable decrease in the local flux downstream of the maximum peak. This drop is higher at lower Reynolds numbers. Therefore, Fig. 11 shows that there will be a Reynolds number that maximises the absorption for each absorber length. This conclusion was also reported by Hofmann and Kuhlmann [26] and García-Rivera et al. [14].

Comparing both methods in the analysed range, the maximum peak is greater considering Fick 1D (Fig. 11(a)) than Higbie 1D (Fig. 11(b)). However, the decrease on absorption rate downstream the maximum peak is lower for Higbie 1D. Therefore, results of the local absorbed

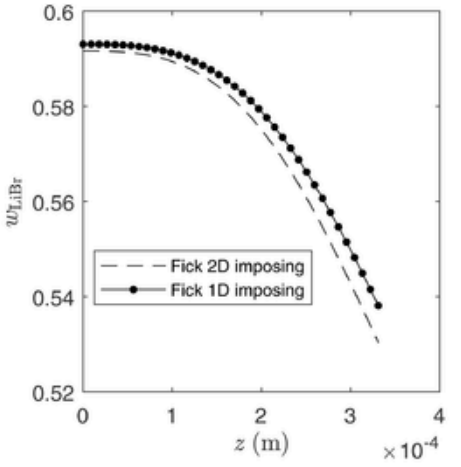

(a) LiBr mass fraction along transversal direction using imposing Fick method at the outlet of the tube ($x = 1.5$ m)

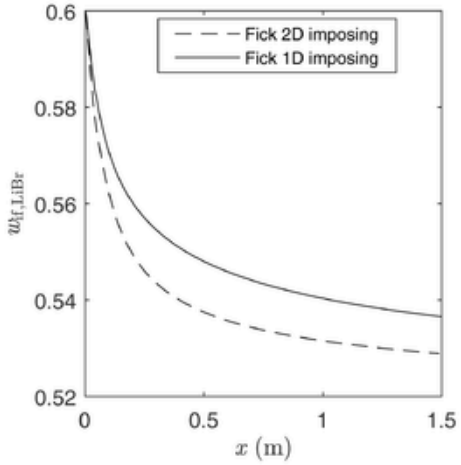

(b) LiBr mass fraction along flow length for imposing Fick method at the interface.

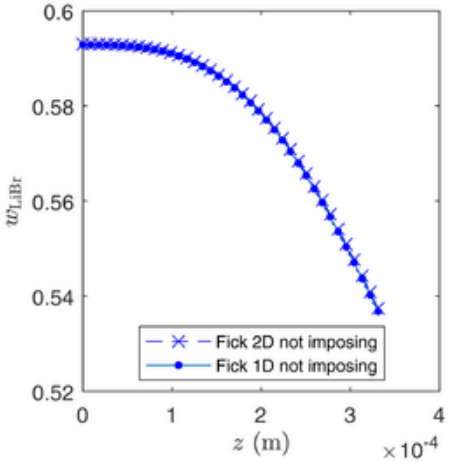

(c) LiBr mass fraction along transversal direction using not imposing Fick method at the outlet of the tube ($x = 1.5$ m).

Fig. 8. Different LiBr mass fraction profiles for different methodologies when $Re = 50$.

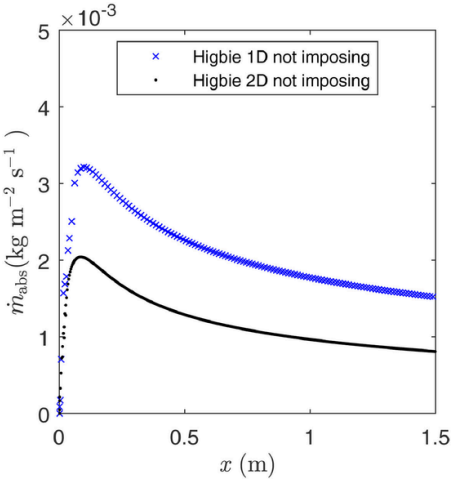

Fig. 9. Comparison of the local absorbed mass flux along the flow length for different diffusion hypothesis using Higbie method when $Re = 50$.

mass flux do not vary that much using Higbie 1D (Fig. 11(b)), which is due to the low impact of absorbed vapour quantity. Thus, it is noted that Fick 1D method is more sensitive to mass fraction changes due to absorption than Higbie 1D.

In the range of this study, notably, the absorption mass flux also depends on the heat transfer in the transversal direction but, however, its impact varies with the Reynolds number. Here, Fig. 12 depicts the absorbed mass flux along the flow length for Fick 1D (Fig. 12(a)) and Higbie 1D (Fig. 12(b)) for two different Reynolds numbers: $Re = 50$ and $Re = 290$, when they are operating under different convection coefficients of the cooling fluid.

Results of Fig. 12 shows that in both methods, the flux increases with higher convection coefficients. Furthermore, the maximum peak is located at a lower flow length when the convective load is higher. This is because, consequent to the convection enhancement, the thermal boundary layer development is faster, and therefore, the same temperature is obtained at a lower flow length. This improvement is higher when $Re = 290$ because of the thicker film thickness.

Also, the impact is higher using Fick 1D (Fig. 12(a)) than Higbie 1D (Fig. 12(b)). The local absorbed flux and the heat generated are higher for Fick 1D. Thus, the higher the mass absorption, the bigger the enhancement due to the convection load. However, the rise from $\bar{h}_{H_2O} = 6000$ Wm^{-2}K^{-1} to $\bar{h}_{H_2O} = 8000$ Wm^{-2}K^{-1} is small. Consequently, the improvement is saturated from a specific cooling load, so it would not be interesting from a design perspective.

Overall, the model results revealed that increasing the convection of the cooling water improves the absorption, although, for the case analysed, this increase is saturated from $\bar{h}_{H_2O} = 6000$ Wm^{-2}K^{-1}. Moreover, this growth is larger for $Re = 290$ than for $Re = 50$.

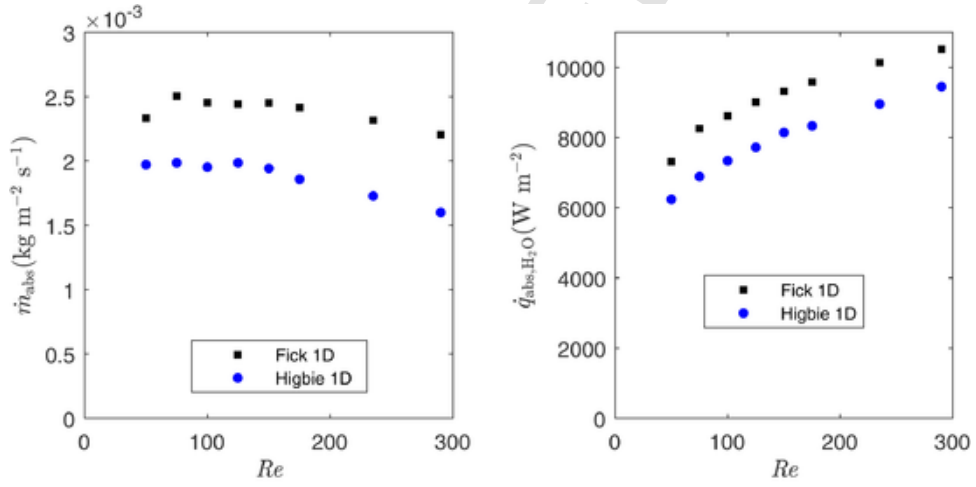

(a) Absorbed mass flux. (b) Absorbed heat flux by the cooling fluid.

Fig. 10. Average results of the numerical model for different Reynolds numbers and methodologies.

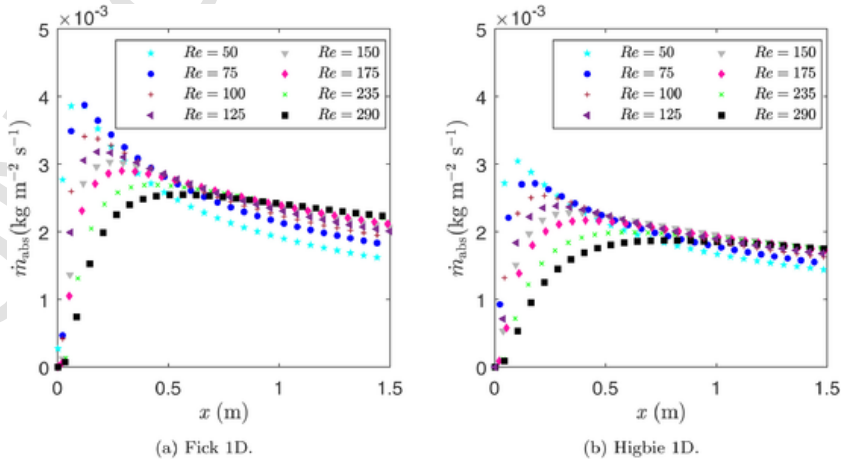

(a) Fick 1D. (b) Higbie 1D.

Fig. 11. Local absorbed mass flux along the flow length for different Reynolds numbers using different methodologies.

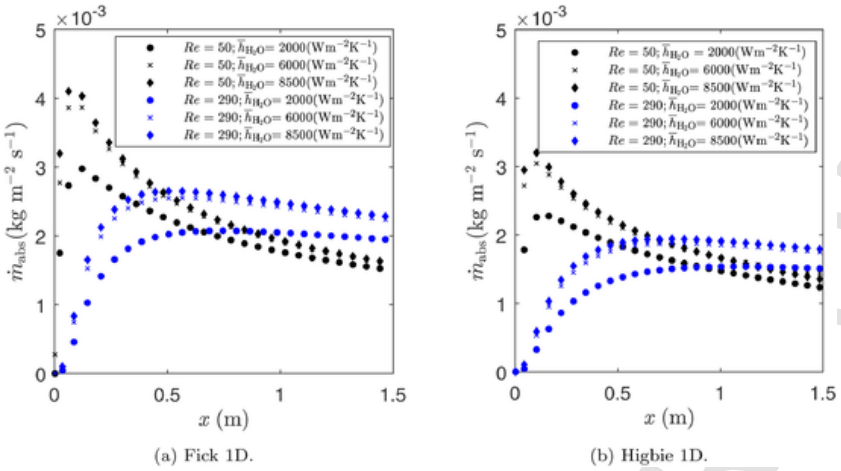

Fig. 12. Local absorbed mass flux along flow length for different methods when $Re = 50$ and $Re = 290$ operating under different convection coefficient values of the cooling fluid.

Finally, the effect of the inlet mass fraction was studied. Both experimental [12,44] and numerical [26,36] researches of the literature have demonstrated a considerable impact of the inlet mass fraction on the absorption. However, studies that analysed the effect in Fick 1D and Higbie 1D are lacking. Therefore, Fig. 13 presents local absorption mass flux evolution over flow length for two different inlet mass fractions ($w_{\text{in,LiBr}} = 0.6$ and $w_{\text{in,LiBr}} = 0.58$), when $Re = 50$ and $Re = 290$ for two different methods to determine the absorption rate: Fick 1D (Fig. 13(a)) and Higbie 1D (Fig. 13(b)).

What is striking about the Fig. 13 is the large impact of the inlet mass fraction on the absorption in this study for both Fick 1D (Fig. 13 (b)) and Higbie 1D (Fig. 13(b)). Only reducing the mass fraction from $w_{\text{in,LiBr}} = 0.6$ to $w_{\text{in,LiBr}} = 0.58$, a fall in the absorption is induced. The decrease is more considerable for Fick 1D. Therefore, as was also evidenced by the analysis of the influence of the Reynolds number of the solution, Fick 1D method is more sensitive to inlet mass fraction alterations. This decrease was also observed by some other experimental studies [12,14,44].

3.5. Comparison of numerical results and experimental studies

As mentioned in Section 1, different formulations in numerical models and analytical calculations were used in the literature. In some cases, model results were compared with experimental data. However, the difference between the considered calculation methodologies and procedures for introducing the absorption flux and the experimental results has not yet been compared. Therefore, the numerical results were analysed and compared considering the same working conditions of the experimental studies. Due to the lack of information on the working conditions and the wettability performance, the studies of Yüksel and Schlünder [52] and Miller and Keyhani [44] were discarded for the comparison. The contrasted works were Medrano et al. [12], Takamatsu et al. [13], and García-Rivera et al. [14], whose operating conditions were described in Table 1.

To evaluate the proposed models, Fig. 14 shows the comparison of the models and the tests of Medrano et al. [12], where the solution was introduced at subcooled conditions (Table 1).

Figure 14 results show that using both Fick 1D and Higbie 1D, the model results agree with the trend of the experimental results. The higher the Reynolds number, the higher the absorbed mass flux. In this case, Fick 1D method shows the best agreement with experiments. In particular, except for $Re = 300$, the rest of the results are within the uncertainty range of the experiments. On the contrary, differences were higher for Higbie 1D method.

The second comparison was made with the experimental results obtained by Takamatsu et al. [13] at equilibrium conditions. Fig. 15 presents the contrast between the experimental tests [13] and the numerical results obtained in this study for two different cooling water inlet temperature conditions: $T_{\text{H}_2\text{O}} = 20\ ^\circ\text{C}$ (Fig. 15(a)) and $T_{\text{H}_2\text{O}} = 25\ ^\circ\text{C}$ (Fig. 15(b)).

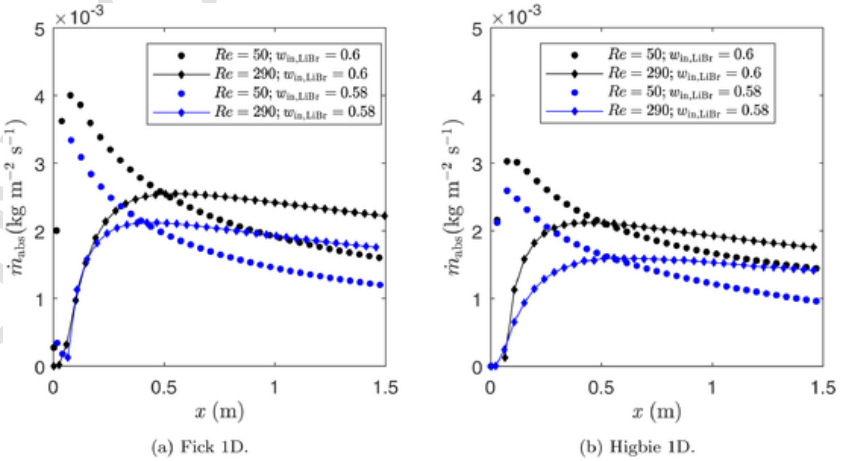

Fig. 13. Results of local absorbed vapour mass flux for different inlet mass fractions ($w_{\text{in,LiBr}} = 0.6$ and $w_{\text{in,LiBr}} = 0.58$) and Reynolds numbers ($Re = 50$ and $Re = 290$), obtained using two different methods.

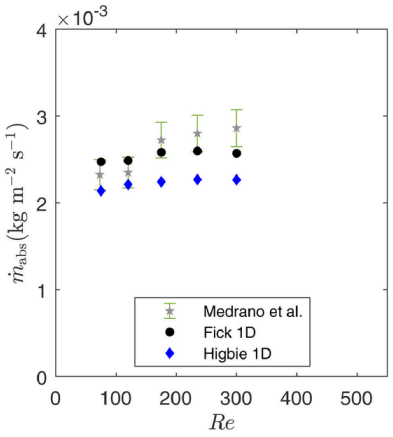

Fig. 14. Comparison of the absorbed vapour mass flux between experimental results from the study by Medrano et al. [12] and numerical results

The results in Fig. 15 illustrate that, similar to that of the comparison with Medrano et al. [12], the results of the model and experimental tests also follow the same trend. In particular, Fick 1D (Fig. 15) is also the one that gives the most similar results to the experimentation of Takamatsu et al. [13]. Almost all of the absorption fluxes obtained with Fick 1D are within the uncertainty range of the measurements (Fig. 15). Besides $Re = 550$ and $T_{H_2O} = 25$ °C, the differences with the others are below 6%.

For Higbie 1D (Fig. 15), the differences between numerical and experimental results were larger. The maximum difference was 20% for the highest Reynolds number.

To conclude the comparison, the difference between the experimental results of García-Rivera et al. [14] and those obtained with the numerical models of this study at equilibrium conditions was examined in Fig. 16. Figure 16(a) shows the difference in the absorbed vapour mass flux, while Fig. 16(b) presents the comparison of the heat flux absorbed by the cooling water.

As in preceding comparisons, the numerical results for both absorbed mass flux and heat flux follow the same trend as the experimental results (Fig. 16). The mass flux absorbed increases with Reynolds number up to $Re \approx 110$, where it starts to decrease with Reynolds num-

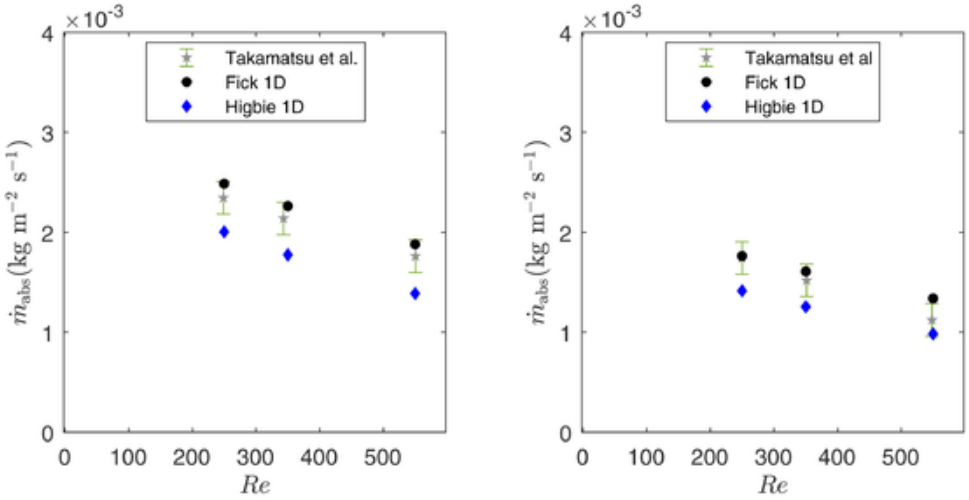

Fig. 15. Comparison of the absorbed vapour mass flux between experimental results from the work of Takamatsu et al. [13] and numerical results, for two different water temperature inlet conditions.

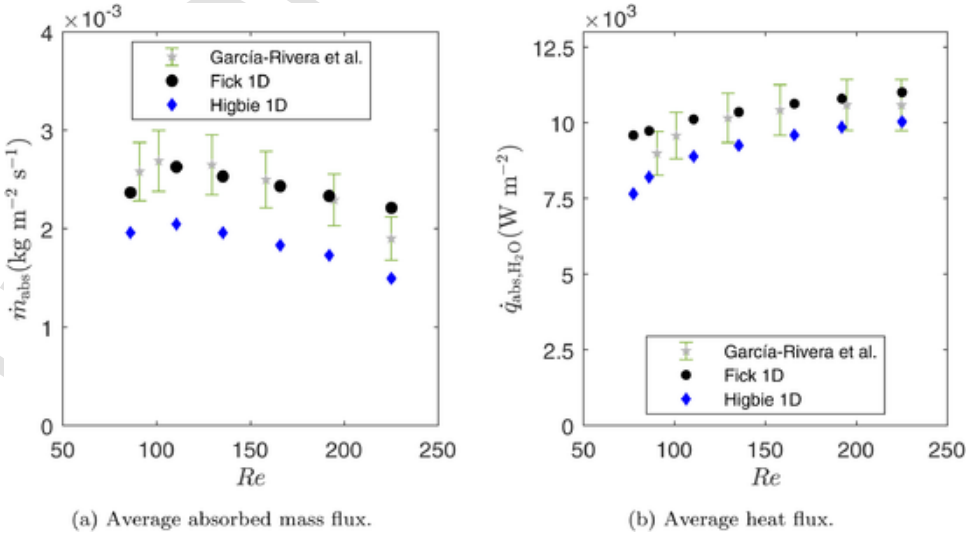

Fig. 16. Comparison between experimental results from the work of García-Rivera et al. [14] and numerical results.

ber (Fig. 16(a)). Thus, both numerical and experimental results indicated that there is an optimal Reynolds number that maximises vapour absorption. Under the working conditions of the analysed absorber, this Reynolds number would have a value of $Re \approx 110$.

For heat flux (Fig. 16(b)), it increases with the Reynolds number, although at high Reynolds numbers, the growth rate decreases in both experimental and numerical results. Furthermore, the results obtained with the Fick 1D method are within the measurement uncertainty. For Higbie 1D, the results differed more from the experimental, although many of them are still within the measurement uncertainty.

Overall, the results obtained using Fick 1D method were closer to the experimental results. Most of these results were within the measurement uncertainty of the experimental tests. The difference between Fick 1D models and experiments may be due to the considered assumptions by this method such as that the vapour absorption does not vary the film thickness and that the velocity is not considered in this method. Moreover, in both inlet subcooling and equilibrium condition cases, the absorption in the model follows the same trend as in the experiments. The results obtained with Higbie 1D also follow the same trend, but the differences with the experimental results were larger. The discrepancy could be attributed to the chosen expression to estimate the contact time (x/u_{max}) in Higbie's equation. Depending on the applied area, there are different methods to determine the contact time, so reformulation of this contact time could even out these differences. In addition, the velocity of the water vapour could also play a role in the variations.

4. Conclusions

This study offers some important insights into the impact of different mathematical formulations, hypothesis, and methodologies used in numerical models to determine and consider the absorption, particularly, on $LiBr - H_2O$ vertical tube-type falling film absorbers. 2D steady two phase flow models using different methodologies to consider absorption were defined to analyse the heat and mass transfer behaviour on the absorber operating at both inlet subcooling and equilibrium conditions. These methodologies were based on three different criteria. The first relates to the way to consider vapour absorption in the model, that is, either imposing thermodynamic equilibrium conditions at the interface, or not imposing, considering the absorption via source terms related to the absorbed mass flux. The second has a relationship with the method to determine the absorption rate. In this study, two different laws were employed– Fick's law and Higbie's law. Finally, the third criterion of the methodology is the hypothesis of the type of diffusion at the interface, which could be 1D or 2D diffusion.

The results of the mesh independence analysis showed that the computational mesh for Higbie's method is less challenging than for Fick. Using this independent mesh, the results of the proposed models were compared with the models of Yoon et al. and Mittermaier et al. using the methodology followed by the authors, showing excellent agreement between them.

The comparison of different methodologies revealed that the methodology to determine and consider absorption changes considerably the absorption performance. Moreover, this analysis found that when equilibrium conditions are imposed, the calculated vapour absorption and the introduced within the solution liquid are distinct when 1D diffusion is assumed. An implication of this is the possibility that the calculated mass flux values and the mass fraction profiles might be contradicted using 1D diffusion assumption in the imposing method. Adding to this, due to the negligible vapour pressure of the LiBr, Fick 1D and Higbie 1D methods without imposition were suggested to analyse the absorption on $LiBr - H_2O$ absorbers. The main reason for excluding Fick 2D without imposition was that the LiBr is non volatile, and therefore, 1D diffusion option would be preferable to describe the absorption phenomenon. Nevertheless, the comparison with Fick 1D revealed that 2D approach could also obtain a good agreement with experiments.

Furthermore, the study of the influence of the operating conditions on the selected methodologies revealed that, although both methods presented similar trends, Fick 1D method is more sensitive to the changes on the convective coefficient and the inlet mass fraction. This may be because the variations of the mass fraction at the interface have a higher impact for Fick 1D. Also, the comparison with the experimental works showed closer results for Fick 1D, where most of the results were within the measurement uncertainty range of the three compared experimental studies. The differences between numerical results using Fick 1D method and experiments may be due to the considered assumptions. However, studying further different contact times and considering the velocity of the water vapour could also make Higbie 1D a suitable method, because of its less computational cost.

Overall, this study proposes a valuable numerical methodology for analysing the local thermal and mass transfer phenomena and for the design of efficient falling film heat exchangers, which will be helpful for developing future numerical models.

CRediT authorship contribution statement

P.F. Arroiabe: Methodology, Software, Validation, Writing – original draft. **Manex Martinez-Agirre:** Conceptualization, Methodology, Writing – review & editing. **M. Mounir Bou-Ali:** Conceptualization, Writing – review & editing, Supervision, Funding acquisition.

Declaration of Competing Interest

None.

Acknowledgements

Authors would like to thank the support of CONVADP (No. KK-2020-00091) and Research Groups (No. IT1009-16) of Basque Government.

References

[1] Eurostat, Energy, transport and environment statistics, 2020 edition, European Commission, 2020, https://doi.org/10.2785/522192.
[2] S. Brückner, S. Liu, L. Miró, M. Radspieler, L.F. Cabeza, E. Lävemann, Industrial waste heat recovery technologies: an economic analysis of heat transformation technologies, Appl. Energy 151 (2015) 157–167, https://doi.org/10.1016/j.apenergy.2015.01.147.
[3] M.R. Islam, Absorption process of a falling film on a tubular absorber: an experimental and numerical study, Appl. Therm. Eng. 28 (11–12) (2008) 1386–1394, https://doi.org/10.1016/j.applthermaleng.2007.10.004.
[4] I. Kyung, K.E. Herold, Y.T. Kang, Experimental verification of H2O/LiBr absorber bundle performance with smooth horizontal tubes, Int. J. Refrig 30 (4) (2007) 582–590, https://doi.org/10.1016/j.ijrefrig.2006.11.005.
[5] A.K. Nagavarapu, S. Garimella, Falling-film absorption around microchannel tube banks, J. Heat Transf. 135 (12) (2013) 122001, https://doi.org/10.1115/1.4024261.
[6] D. Bredow, P. Jain, A. Wohlfeil, F. Ziegler, Heat and mass transfer characteristics of a horizontal tube absorber in a semi-commercial absorption chiller, Int. J. Refrig 31 (7) (2008) 1273–1281, https://doi.org/10.1016/j.ijrefrig.2008.01.016.
[7] D.S. Kim, C.A. Infante Ferreira, Analytic modelling of a falling film absorber and experimental determination of transfer coefficients, Int. J. Heat Mass Transf. 52 (21–22) (2009) 4757–4765, https://doi.org/10.1016/j.ijheatmasstransfer.2009.05.014.
[8] D.S. Kim, C.A. Infante Ferreira, Flow patterns and heat and mass transfer coefficients of low Reynolds number falling film flows on vertical plates: effects of a wire screen and an additive, Int. J. Refrig 32 (1) (2009) 138–149, https://doi.org/10.1016/j.ijrefrig.2008.08.005.
[9] J.I. Yoon, E. Kim, K.H. Choi, W.S. Seol, Heat transfer enhancement with a surfactant on horizontal bundle tubes of an absorber, Int. J. Heat Mass Transf. 45 (4) (2001) 735–741, https://doi.org/10.1016/S0017-9310(01)00202-2.
[10] T. Wen, L. Lu, H. Zhong, C. Dong, Experimental and numerical study on the regeneration performance of LiCl solution with surfactant and nanoparticles, Int. J. Heat Mass Transf. 127 (2018) 154–164, https://doi.org/10.1016/j.ijheatmasstransfer.2018.07.098.
[11] H. Zhang, D. Yin, S. You, W. Zheng, S. Wei, Experimental investigation of heat and

mass transfer in a LiBr-H2O solution falling film absorber on horizontal tubes: comprehensive effects of tube types and surfactants, Appl. Therm. Eng. 146 (July 2018) (2019) 203–211, https://doi.org/10.1016/j.applthermaleng.2018.09.127.
[12] M. Medrano, M. Bourouis, A. Coronas, Absorption of water vapour in the falling film of water-lithium bromide inside a vertical tube at air-cooling thermal conditions, Int. J. Therm. Sci. 41 (9) (2002) 891–898, https://doi.org/10.1016/S1290-0729(02)01383-2.
[13] H. Takamatsu, H. Yamashiro, N. Takata, H. Honda, Vapor absorption by LiBr aqueous solution in vertical smooth tubes, Int. J. Refrig 26 (6) (2003) 659–666, https://doi.org/10.1016/S0140-7007(03)00038-0.
[14] E. García-Rivera, J. Castro, J. Farnós, A. Oliva, Numerical and experimental investigation of a vertical LiBr falling film absorber considering wave regimes and in presence of mist flow, Int. J. Therm. Sci. 109 (2016) 342–361, https://doi.org/10.1016/j.ijthermalsci.2016.05.029.
[15] J.D. Killion, S. Garimella, A critical review of models of coupled heat and mass transfer in falling-film absorption, Int. J. Refrig 24 (8) (2001) 755–797.
[16] T. Meyer, Analytical solution for combined heat and mass transfer in laminar falling film absorption with uniform film velocity - Diabatic wall boundary, Int. J. Heat Mass Transf. 80 (2015) 802–811, https://doi.org/10.1016/j.ijheatmasstransfer.2014.09.049.
[17] V.E. Nakoryakov, N.I. Grigoryeva, Nonisothermal absorption in thermotransformers, J. Eng. Thermophys. 19 (4) (2010) 196–271, https://doi.org/10.1134/S1810232810040028.
[18] P. Fernandez de Arroiabe, A. Martinez-Urrutia, X. Peña, M. Martinez-Agirre, M.M. Bou-Ali, Influence of the contact angle on the wettability of horizontal-tube falling films in the droplet and jet flow modes, Int. J. Refrig 90 (2018) 12–21, https://doi.org/10.1016/j.ijrefrig.2018.04.003.
[19] Q. Qiu, C. Meng, S. Quan, W. Wang, 3-D simulation of flow behaviour and film distribution outside a horizontal tube, Int. J. Heat Mass Transf. 107 (2017) 1028–1034, https://doi.org/10.1016/j.ijheatmasstransfer.2016.11.009.
[20] T. Wen, Y. Luo, L. Lu, W. He, Enhancing the falling film dehumidification performance from the prospective of CFD simulation, Int. J. Heat Mass Transf. 151 (2020) 119459, https://doi.org/10.1016/j.ijheatmasstransfer.2020.119459.
[21] Y. Shi, G. Chen, Q. Wang, Q. Chen, Simulation on falling film absorption based on lattice Boltzmann method at moderate Reynolds number, Int. J. Heat Mass Transf. 128 (2019) 991–998, https://doi.org/10.1016/j.ijheatmasstransfer.2018.09.036.
[22] D. Yu, J. Chung, S. Moghaddam, Parametric study of water vapor absorption into a constrained thin film of lithium bromide solution, Int. J. Heat Mass Transf. 55 (21–22) (2012) 5687–5695, https://doi.org/10.1016/j.ijheatmasstransfer.2012.05.064.
[23] Y. Chen, R. Cao, J. Wu, Z. Yi, G. Ji, Alternate heat and mass transfer absorption performances on staggered tube bundle with M-W corrugated mesh guider inserts, Int. J. Refrig 66 (2016) 10–20, https://doi.org/10.1016/j.ijrefrig.2015.10.034.
[24] N. Giannetti, A. Rocchetti, S. Yamaguchi, K. Saito, Heat and mass transfer coefficients of falling- film absorption on a partially wetted horizontal tube, Int. J. Therm. Sci. 126 (December 2017) (2018) 56–66, https://doi.org/10.1016/j.ijthermalsci.2017.12.020.
[25] P. Fernandez de Arroiabe, A. Martinez-Urrutia, X. Peña, M. Martinez-Agirre, M. Mounir Bou-Ali, On the thermodiffusion effect in vertical plate heat exchangers, Eur. Phys. J. E 42 (7) (2019) 85, https://doi.org/10.1140/epje/i2019-11850-7.
[26] E. Hofmann, H.C. Kuhlmann, On the optimum mass transfer of flat absorbing falling films, Int. J. Heat Mass Transf. 55 (25–26) (2012) 7686–7697, https://doi.org/10.1016/j.ijheatmasstransfer.2012.07.074.
[27] M.L. Yüksel, E.U. Schlünder, Heat and mass transfer in non-isothermal absorption of gases in falling liquid films Part II: theoretical description and numerical calculation of turbulent falling film heat and mass transfer, Chem. Eng. Process. 22 (4) (1987) 203–213, https://doi.org/10.1016/0255-2701(87)85003-1.
[28] S.M. Hosseinnia, M. Naghashzadegan, R. Kouhikamali, CFD simulation of adiabatic water vapor absorption in large drops of water-LiBr solution, Appl. Therm. Eng. 102 (2016) 17–29, https://doi.org/10.1016/j.applthermaleng.2016.03.144.
[29] R. Higbie, The Rate of Absorption of a Pure Gas into a Still Liquid during Short Periods of Exposure, University of MICHIGAN, 1934.
[30] D. Sebastia-saez, S. Gu, M. Ramaioli, Effect of the contact angle on the morphology, residence time distribution and mass transfer into liquid rivulets : a CFD study, Chem. Eng. Sci. 176 (2018) 356–366, https://doi.org/10.1016/j.ces.2017.09.046.
[31] T. Wen, Y. Luo, W. He, W. Gang, L. Sheng, Development of a novel quasi-3D model to investigate the performance of a falling film dehumidifier with CFD technology, Int. J. Heat Mass Transf. 132 (2019) 431–442, https://doi.org/10.1016/j.ijheatmasstransfer.2018.12.027.
[32] C. Albert, H. Marschall, D. Bothe, Direct numerical simulation of interfacial mass transfer into falling films, Int. J. Heat Mass Transf. 69 (2014) 343–357, https://doi.org/10.1016/j.ijheatmasstransfer.2013.10.025.
[33] M. Mittermaier, P. Schulze, F. Ziegler, A numerical model for combined heat and mass transfer in a laminar liquid falling film with simplified hydrodynamics, Int. J. Heat Mass Transf. 70 (2014) 990–1002, https://doi.org/10.1016/j.ijheatmasstransfer.2013.11.075.
[34] J. Castro, L. Leal, C.D. Pérez-Segarra, P. Pozo, Numerical study of the enhancement produced in absorption processes using surfactants, Int. J. Heat Mass Transf. 47 (14–16) (2004) 3463–3476, https://doi.org/10.1016/j.ijheatmasstransfer.2004.01.012.
[35] S.M. Hosseinnia, M. Naghashzadegan, R. Kouhikamali, Numerical study of falling film absorption process in a vertical tube absorber including Soret and Dufour effects, Int. J. Therm. Sci. 114 (2017) 123–138, https://doi.org/10.1016/j.ijthermalsci.2016.11.006.
[36] J.I. Yoon, T.T. Phan, C.G. Moon, P. Bansal, Numerical study on heat and mass transfer characteristic of plate absorber, Appl. Therm. Eng. 25 (14–15) (2005) 2219–2235, https://doi.org/10.1016/j.applthermaleng.2005.01.004.
[37] L. Harikrishnan, M.P. Maiya, S. Tiwari, Investigations on heat and mass transfer characteristics of falling film horizontal tubular absorber, Int. J. Heat Mass Transf. 54 (11–12) (2011) 2609–2617, https://doi.org/10.1016/j.ijheatmasstransfer.2011.01.024.
[38] V. Subramaniam, S. Garimella, From measurements of hydrodynamics to computation of species transport in falling films, Int. J. Refrig 32 (4) (2009) 607–626, https://doi.org/10.1016/j.ijrefrig.2009.02.008.
[39] C.W. Hirt, B.D. Nichols, Volume of fluid (VOF) method for the dynamics of free boundaries, J. Comput. Phys. 39 (1) (1981) 201–225 https://doi.org/10.1016/0021-9991(81)90145-5.
[40] T. Wen, L. Lu, Y. Luo, Review on the fundamentals and investigations of falling film dehumidification/absorption refrigeration based on CFD technology, Int. J. Heat Mass Transf. 171 (2021) 121042, https://doi.org/10.1016/j.ijheatmasstransfer.2021.121042.
[41] W. Nusselt, Die Oberflaechenkondensation des Wasserdampfes, Zeitschrift des Vereines Deutscher Ingenieur 60 (27) (1916) 541–546.
[42] F. Dittus, L. Boelter, Heat transfer in automobile radiators of the tubular type. University of California Press, Berkeley, 2, Univ. Calif. Publ. Eng., 1930, pp. 443–461.
[43] M. Patterson, H. Perez-Blanco, Numerical fits of the properties of lithium-bromide water solutions, ASHRAE Annual Meeting, 1988, pp. 2059–2077 http://www.osti.gov/energycitations/product.biblio.jsp?osti_id=7077040.
[44] W.a. Miller, M. Keyhani, The correlation of simultaneous heat and mass transfer experimental data for aqueous lithium bromide vertical falling film absorption, J. Sol. Energy Eng. 123 (1) (2001) 30, https://doi.org/10.1115/1.1349550.
[45] I. Haar, J. Gallaguer, J. Kellk, Steam Tables, Mc Graw Hill, 1984.
[46] Z. Yuan, K.E. Herold, Thermodynamic properties of aqueous lithium bromide using a multiproperty free energy correlation, HVAC&R Res. 11 (3) (2005) 377–393, https://doi.org/10.1080/10789669.2005.10391144.
[47] J.U. Brackbill, D.B. Kothe, C. Zemach, A continuum method for modeling surface tension, J. Comput. Phys. 100 (2) (1992) 335–354, https://doi.org/10.1016/0021-9991(92)90240-Y.
[48] B. Ziegler, C. Trepp, Equation of state for ammonia-water mixtures, Int. J. Refrig 7 (2) (1984) 101–106, https://doi.org/10.1016/0140-7007(84)90022-7.
[49] M. Mittermaier, F. Ziegler, The impact of viscosity on the combined heat, mass and momentum transfer in laminar liquid falling films, Heat Mass Transf./Waerme- und Stoffuebertragung (2017) 1–17, https://doi.org/10.1007/s00231-017-2219-9.
[50] E.L. Cussler, Fundamentals of mass transfer, Diffusion, 2007, pp. 237–273 http://ebooks.cambridge.org/ref/id/CBO9780511805134A076, https://doi.org/10.1017/CBO9780511805134.010.
[51] S.V. Patankar, Numerical Heat Transfer and Fluid Flow, Hemisphere Pub. Corp, Washington, 1980.
[52] M.L. Yüksel, E.U. Schlünder, Heat and mass transfer in non-isothermal absorption of gases in falling liquid films. Part I: experimental determination of heat and mass transfer coefficients, Chem. Eng. Process. 22 (4) (1987) 193–202, https://doi.org/10.1016/0255-2701(87)85002-X.